02

Phonon spectrum and elastic properties of $Gd_2Sn_2O_7$: *ab initio* calculation

© V.A. Chernyshev[1], K.I. Glukhov[1], P.A. Zayats[2]

[1] Ural Federal University after the first President of Russia B.N. Yeltsin, Yekaterinburg, Russia
[2] M.N. Mikheev Institute of Metal Physics, Ural Branch, Russian Academy of Sciences, Yekaterinburg, Russia

e-mail: vladimir.chernyshev@urfu.ru

Received January 24, 2024
Revised June 10, 2024
Accepted June 22, 2024

The phonon spectrum of gadolinium stannate $Gd_2Sn_2O_7$ was calculated within the *ab initio* approach. The frequencies and types of phonon modes active in infrared absorption and Raman scattering were determined. The degree of ion participation in phonon modes was determined from the analysis of displacement vectors that was obtained in the first-principles calculation. The elastic constants and hardness of $Gd_2Sn_2O_7$ were calculated. The effect of hydrostatic pressure on the frequencies of fundamental vibrations was studied. The calculations were carried out within the MO LCAO approach with hybrid functionals that take into account the contribution of nonlocal exchange in the Hartree-Fock formalism. Our results also demonstrate the possibility of using a pseudopotential to describe the inner shells of a rare-earth ion.

Keywords: rare earth stannates, phonons, elastic constants, hybrid functionals.

DOI: 10.61011/EOS.2024.07.59644.5781-24

1. Introduction

Rare-earth (RE) pyrochlores $R_2M_2O_7$ (R — RE ion, M — Ti, Ge, Zr, Sn, Mo) have a variety of properties that are used to develop new materials. They may be potentially used as solid electrolytes with oxygen ion conductivity [1,2], are used in thermal protective coatings [3,4], and are considered as promising materials for radioactive waste immobilization [5,6]. They receive attention as luminescent materials [7–13], and may be activated by other RE ions [14]. It is important to develop a technique to calculate a set of properties of these materials as a single *ab initio* approach. It is of interest within the single *ab initio* approach to study the crystal structure, band structure, phonon spectrum, and elastic properties of RE pyrochlores. It is also important to study external impacts such as pressure on the RE pyrochlore properties.

Density functional theory calculation using the exchange-correlation functional that takes into account the nonlocal exchange contribution is currently most adequate for this purpose. The state-of-the-art theory does not include a universal exchange-correlation functional, therefore to choose one among the existing functionals, calculated data shall be compared with the available experimental data. Among RE pyrochlores $R_2M_2O_7$, most of the experimental data available in the literature pertains to RE stannates $R_2Sn_2O_7$ ($R = \mathrm{La} - \mathrm{Lu}$). Their crystalline structure [15,16], Raman scattering (RS) and infrared (IR) absorption spectra [16–18], elastic constants and Vickers hardness [15] were examined. There is no experimental band gap (BG) data for RE stannates in the literature, except gadolinium stannate $Gd_2Sn_2O_7$ whose band gap was measured quite recently [19]. This makes $Gd_2Sn_2O_7$ a convenient model for choosing an exchange-correlation functional and developing a calculation technique. Pyrochlore structure has high symmetry (space group $Fd\bar{3}m$), but two formula units in a primitive cell, $Z = 2$, i.e. 22 ions, including four RE ions. Simulation of such structure using the *ab initio* approach is very computer-intensive. Calculation of phonon spectrum and elastic constants appears to be particularly computer-intensive. To make this problem computer-solvable, a pseudopotential method shall be used to describe inner electron shells of Sn and RE ion. It is important to check whether a „long“ pseudopotential may be used for the RE ion to replace its inner shells up to $4f$, inclusive, when simulating the RE stannate lattice structure and behavior. In this case we will get a closed shell system that will allow using a spin-limited calculation and significant time and resource saving. $Gd_2Sn_2O_7$ is also attractive for such check because Gd^{3+} has a largest number of unpaired electrons on the $4f$-shell ($S = 7/2$) among all RE ions. Moreover, $Gd_2Sn_2O_7$ has a variety of properties, can be potentially used for actinide immobilization [6], and is considered as a promising luminescent material for Yb^{3+}/Er^{3+}codoping [20]. Therefore the study of its phonon spectrum, elastic properties, pressure effect on $Gd_2Sn_2O_7$ is of particular interest.

2. Calculation methods

$Gd_2Sn_2O_7$ has a pyrochlore structure, space group (no. 227). In the pyrochlore structure, ions in the lattice cell are in the following positions: Sn — 16*c* (0, 0, 0), Gd — 16*d* (1/2, 1/2, 1/2). Oxygen is in two positions: O1 — 48*f* (*x*, 1/8, 1/8), O2 — 8*b* (3/8, 3/8, 3/8).

Calculations were conducted within the density functional theory (DFT). We used CRYSTAL17 program [21] designed to simulate periodic structures in line with the MOLCAO approach („molecular orbital — linear combination of atomic orbitals"). An all-electron basis [22] with polarization *d*-orbitals was used for oxygen. To describe inner shells of tin, $n = 1-3$, a relativistic pseudopotential was used, while the outer shells — $4s^24p^64d^{10}5s^25p^2$ involved in chemical bonding were described through a valence basis set [23] with polarization *d*- and *f*-orbitals. To describe inner shells of gadolinium, a quasi-relativistic pseudopotential ECPnMWB (ECP — effective core potential; *n* is the number of inner electrons replaced with the pseudopotential) was used. Calculations were conducted within the study both with explicit consideration of the 4*f*-shell of gadolinium and with replacement of this shell with a pseudopotential. A pseudopotential with $n = 28$ or $n = 53$ was used, respectively. The outer shell of gadolinium were described explicitly through the TZVP type valence basis sets. Pseudopotentials and valence basis sets used for gadolinium are available on the web-site [24].

When solving a system of one-electron Kohn-Sham equations, the accuracy of self-consistent field calculation was 10^{-7} a. u. The accuracy of two-electron integral calculation was at least 10^{-8} a.u. Integration over the Brillouin zone was carried out using the Monkhorst-Pack scheme with the *k*-point $8 \times 8 \times 8$ grid

Crystalline structure relaxation considers that forces acting on atoms in a stationary point on the potential energy surface shall be equal to zero. Optimization is deemed to be completed when the forces on atoms become lower than the threshold. To evaluate the magnitude of forces at each optimization step, CRYSTAL calculates an rms energy gradient and absolute value of its largest component. Their threshold values were set to 0.00030 a. u. and 0.00045 a. u., respectively. Besides the smallness of forces, CRYSTAL uses another criterium — smallness of ionic displacements with respect to the previous step. Displacement magnitudes are evaluated using the rms and absolute values of the largest component. Their threshold values were equal to 0.0012 a.u. and 0.0018 a.u. Optimization was deemed to be completed if all four conditions defining the smallness of forces and the smallness of displacements with respect of the previous step were performed simultaneously.

In CRYSTAL, the phonon spectrum is calculated in the harmonic approximation with dynamical matrix computation. The first and second derivatives with respect to ionic displacements are calculated analytically and numerically, respectively [25]. Ionic displacements in the numerical calculation of the second derivative are set to 0.003 Å. Intensity of the IR and Raman spectra is calculated in CRYSTAL [26] using the Born charges [27]. For elastic constant calculation, CRYSTAL calculates the second derivatives of the cell energy with respect to deformations [26,28]:

$$C_{ij} = \frac{1}{V}\left[\frac{\partial^2 E}{\partial \varepsilon_i \partial \varepsilon_j}\right]. \quad (1)$$

The first derivatives in (1) are calculated analytically, the second derivatives are calculated numerically: the deformation ε_i is superimposed on the lattice cell, and the crystalline structure relaxes at the superimposed deformation.

The calculation sequence was as follows. The crystalline structure was optimized first in the study. Then, a phonon spectrum calculation (in Γ-point) or elastic constant calculation was conducted for the optimized crystalline structure.

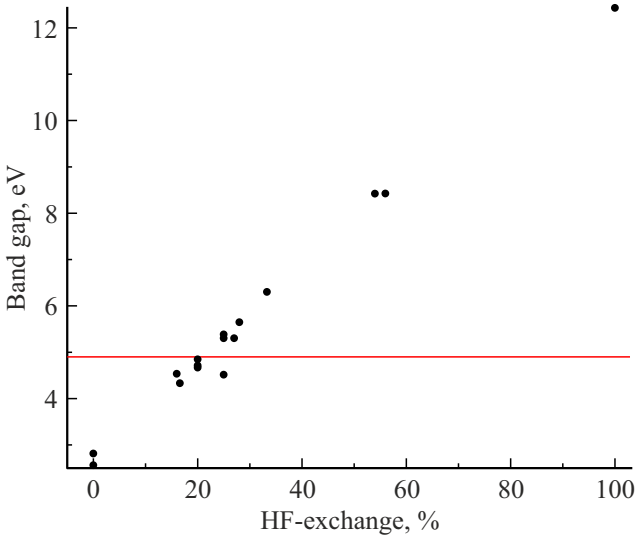

Figure 1. Dependence of the band gap on the Hartree-Fock exchange percentage. The horizontal red line shows the experimental band gap value [19].

3. Development of the approach

For the purpose of calculation, it was necessary to select a DFT functional describing the gadolinium stannate structure, phonon spectrum and elastic properties most adequately. Then check if it is possible to use a „long" pseudopotential replacing the inner shell up to 4*f*, inclusive, to describe the RE ion inner shells. In case when the RE ion inner shell up to 4*f*, inclusive, may be replaced with a pseudopotential without degrading the crystal property description, we'll get a system where all shells will be filled and we won't need to use spin-polarized DFT, which will significantly reduce the computational burden.

During the study, a series of crystalline structure and band gap (BG) calculations were performed for $Gd_2Sn_2O_7$ with various DFT functionals. A set of hybrid functionals

Table 1. Lattice constant and band gap of $Gd_2Sn_2O_7$. The percentage of the nonlocal Hartree-Fock exchange contribution is shown in brackets after the name of the functional in the „Functional“ column. Difference from the experimental data is shown in the „Δ“ columns

Functional (% of Hartree-Fock exchange)	Lattice constant, Å		Band gap, eV	
	calculation	Δ	calculation	Δ
BLYP (0)	10.7440	0.28	2.60	−2.3
PBE (0)	10.6399	0.17	2.81	−2.1
B1WC (16)	10.4791	0.02	4.54	−0.4
WC1LYP (16.6)	10.5746	0.11	4.33	−0.6
B3LYP (20)	10.6210	0.16	4.67	−0.2
B3PW (20)	10.5455	0.09	4.71	−0.2
B97H (20)	10.5993	0.14	4.85	−0.1
HSE06 (25)	10.5234	0.06	4.52	−0.4
PBE0 (25)	10.5186	0.05	5.39	0.5
BESOL0 (25)	10.4457	−0.01	5.30	0.4
M06 (27)	10.5516	0.09	5.30	0.4
M05 (28)	10.6051	0.15	5.65	0.8
PBE0-13 (33.3)	10.4843	0.02	6.30	1.4
M062X (54)	10.5346	0.07	8.42	3.5
M052X (56)	10.5036	0.04	8.42	3.5
M06HF (100)	10.4652	0.01	12.43	7.5
Experiment [16]	10.4603	–	–	–
Experiment [15]	10.4599	–	–	–
Experiment [19]	–	–	4.9	–

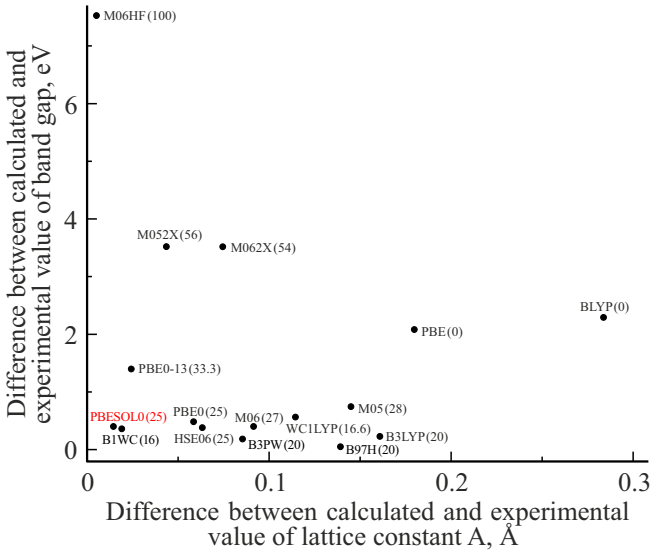

Figure 2. Difference between the calculated and experimental lattice constant and band gap. The calculations were performed using various DFT functionals. The Hartree-Fock exchange percentage is shown in brackets after the name of functional.

considering the unlocal Hartree-Fock exchange contribution and several most widely used non-hybrid functionals were addressed.

The calculated lattice constant and band gap are shown in Table 1. The band gap was calculated from the estimated „highest occupied molecular orbital–lowest unoccupied molecular orbital“ (HOMO–LUMO). The calculations show

Table 2. Band gap of $Gd_2Sn_2O_7$. Calculation with the explicitly considered $4f$-shell and calculation when the $4f$-shell is replaced with a pseudopotential. (Calculation with the PBE0.

Consideration of the $4f$-shell	Band gap, eV
$4f$-shell considered explicitly	5.5
$4f$-shell is replaced by a pseudopotential	5.4

that almost all functionals overestimate the lattice constant compared with the experiment [15,16], but the hybrid functionals reproduce the lattice significantly better that non-hybrid functionals. Maximum deviation from the lattice constant for hybrid and non-hybrid functionals is $\sim 1.5\%$ and $\sim 2.7\%$, respectively. Figure 1 shows the dependence of the calculated band gap on the percentage of Hartree-Fock exchange contribution in the functional. Note that the band gap almost linearly depends on the Hartree-Fock exchange percentage. Experimental data on the band gap of $Gd_2Sn_2O_7$ — 4.9 eV has been only recently reported in the literature [19]. As shown in Figure 1, the minimum difference between the experimental data simultaneously in terms of the lattice constant and band gap is provided by hybrid functionals, for example, PBE0 and its modification for PBESOL0 crystals, and B1WC. This is illustrated in Figure 2. In Figure 2, differences between the calculated and experimental lattice constants and between the calculated and experimental BGs are plotted on the x axis and y

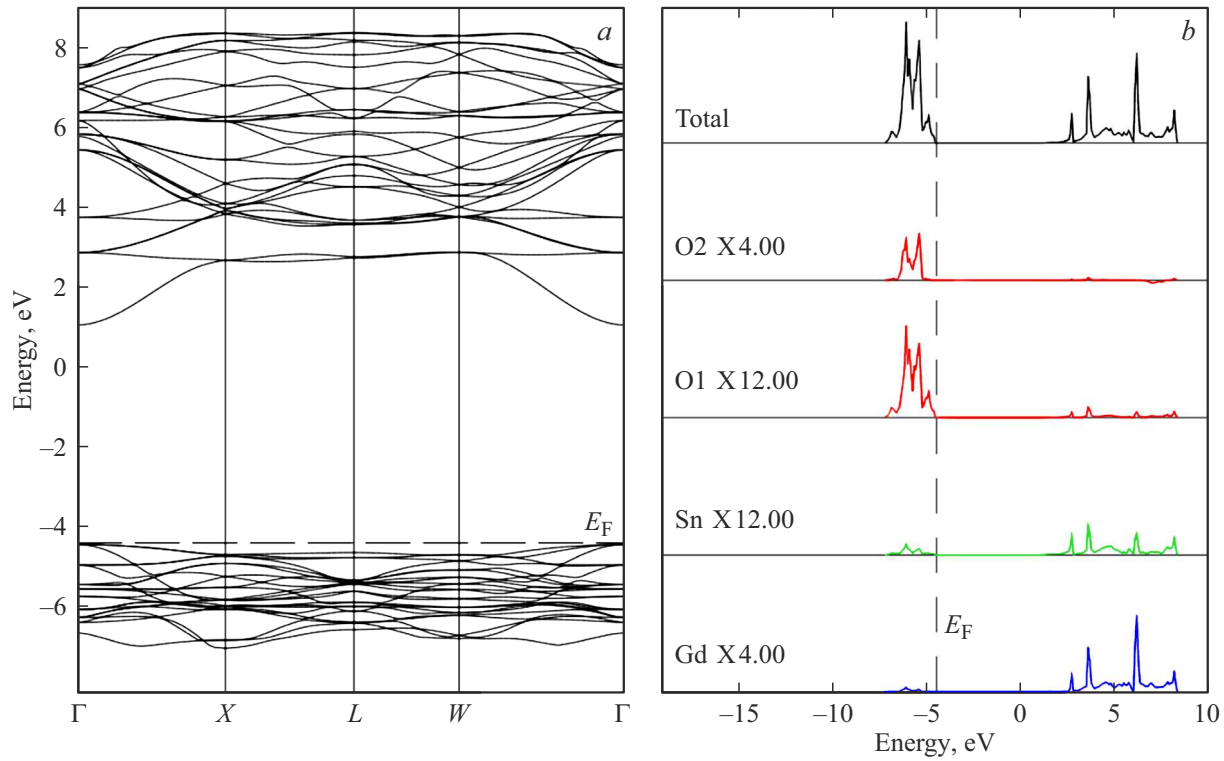

Figure 3. The band structure and density of electronic states of $Gd_2Sn_2O_7$, when the $4f$-shell of gadolinium is replaced by a pseudopotential. Calculation with the PBESOL0.

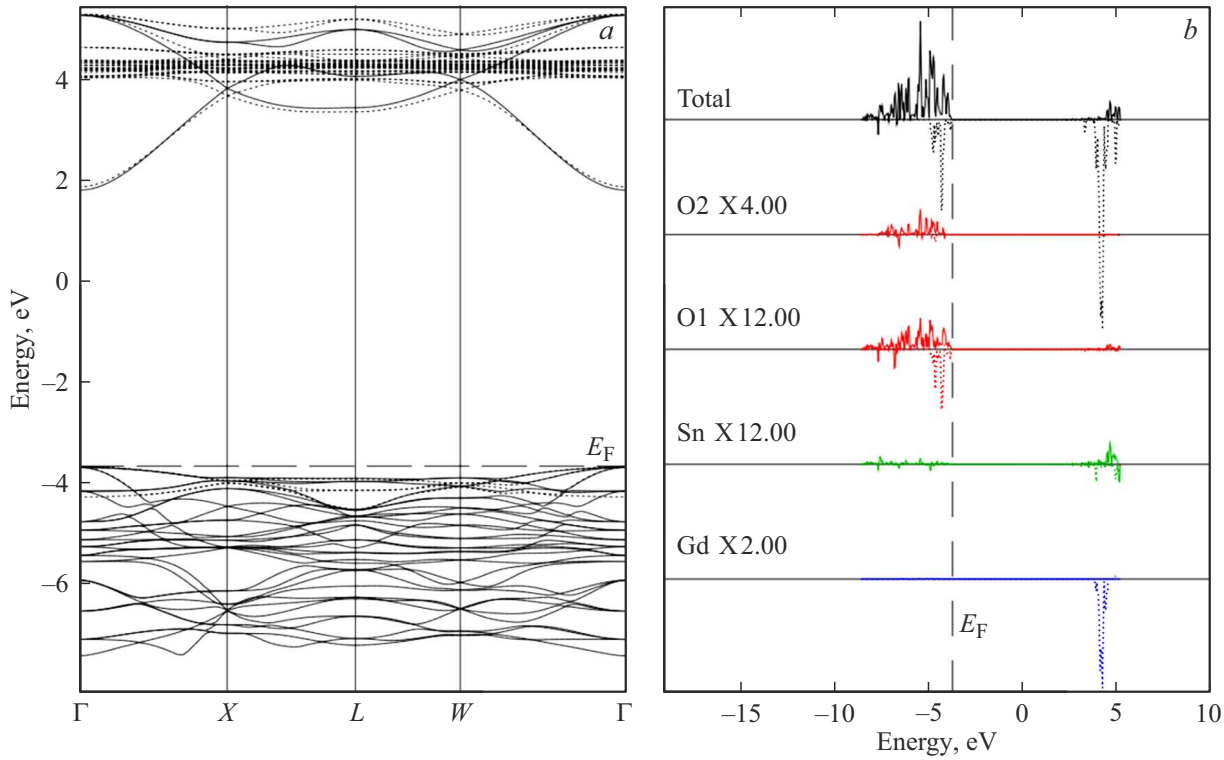

Figure 4. The band structure and density of electronic states of $Gd_2Sn_2O_7$, when the $4f$-shell of gadolinium is explicitly considered. Calculation with the PBE0.

Table 3. Elastic constants of $Gd_2Sn_2O_7$, GPa. Calculation when the $4f$-shell is explicitly considered and replaced by apseudopotential

Elastic constant	$4f$-shell explicitly considered	$4f$-shell replaced by pseudopotential	Experiment [15]	Difference between the calculation and experiment, %	
				$4f$-shell explicitly considered	$4f$-shell replaced by a pseudopotential
C_{11}	332	313	334	−0.6	−6.3
C_{12}	110	110	122	−9.8	−9.8
C_{44}	103	98	106	−2.8	−7.5

Table 4. Elastic moduli and Vickers hardness (GPa)

Elastic moduli	Calculation scheme	$4f$-shell explicitly considered	$4f$-shell replaced by a pseudopotential	Difference between the calculation with and without the $4f$-shell, %
Bulk modulus (B)	Voigt	184	177	−3.8
	Reuss	184	177	−3.8
	Hill	184	177	−3.8
Young-modulus	Voigt	268	251	−6.3
	Reuss	268	251	−6.3
	Hill	268	251	−6.3
Shear modulus (G)	Voigt	107	99	−7.5
	Reuss	106	99	−6.6
	Hill	106	99	−6.6
Vickers hardness H_V		13.4	12.3	−8.2

Table 5. RS-active modes $Gd_2Sn_2O_7$

Type	Experiment [17]	Experiment [18]	Calculation		
			$4f$-shell considered explicitlly		$4f$-shell replaced by a pseudopotential
			(PBE0)	(PBE0-D3)	(PBE0)
F_{2g}	310	310	324	335	310
E_g	346	348	359	370	349
F_{2g}	415	415	444	454	416
A_{1g}	502	502	524	534	506
F_{2g}	530	535	583	594	541
F_{2g}	–	741	760	778	742
Mean difference with experiment, %			5.1	7.7	0.4

axis, respectively. Thus, the functional that is closer to the origin of coordinates is more adequate for stannates. A series of calculations with the PBESOL0 functional and other hybrid functionals conducted previously for RE zirconates has shown that the PBESOL0 functional for some IR modes provides an intensity that differs by two orders of magnitude from those values that provide other hybrid functionals. The PBE0 functional is more proven by various research teams than the B1WC, therefore this study will use the PBE0. Note that the selection of functionals for $BaSnO_3$ in [29] has shown the advantages of the PBE0 functional.

Two series of calculations were conducted for $Gd_2Sn_2O_7$ — with explicit consideration of the $4f$-shell of gadolinium and when the shell is replaced by a pseudopotential. The calculation predicts the same band gap when the $4f$-shell of gadolinium is explicitly considered and replaced by a pseudopotential (Figure 3, 4, Table 2). Both calculations predict the direct band ($\Gamma-\Gamma$), which agrees with the experimental data [19]. Note that the explicit consideration

of the $4f$-shell improves the lattice constant reproduction by several hundredths of angstrom. The calculation when the $4f$-shell was replaced by a pseudopotential provided a lattice constant of 10.52, the calculation with explicit consideration of the $4f$-shell provided -10.48, while the experiment result was -10.46 Å. (Calculations with the PBE0.)

Calculated elastic constants for the case when the $4f$-shell was explicitly considered and replaced by a pseudopotential are shown in Table 3. Calculation with the explicitly considered $4f$-shell somewhat improves the agreement with the experiment for the elastic moduli, but the calculation time is more than doubled, i.e. the explicit consideration of the $4f$-shell implies high computational burden.

The calculated elastic constants were used to calculate the elastic moduli and Vickers hardness (Table 4). The Vickers hardness was calculated using an empirical equation offered in [30] based on the fact that correlations between the Vickers hardness and ratio of shear and bulk moduli G/B were observed for polycrystalline samples. It is written as

$$H_V = 0.92\left(\frac{G}{B}\right)^{1.137} G^{0.708}, \qquad (2)$$

where G is the shear modulus, B is the Hill bulk modulus. Equation (2) was successfully used to describe the hardness of some compounds with ionic and covalent bonds, $M\mathrm{ClO}_3$ and $M\mathrm{ClO}_4$ (M = Li, K, Na) [31].

Difference between the calculated elastic properties when the $4f$-shell of gadolinium was explicitly considered and replaced by a pseudopotential is minor (Table 3, 4).

Calculated phonon spectrum of $Gd_2Sn_2O_7$ with the $4f$-shell of gadolinium explicitly considered and replaced by a pseudopotential are listed in Table 5, 6. The phonon spectrum calculation has shown that the RS and IR mode frequencies are described better when the $4f$-shell is replaced by a pseudopotential. This improvement is associated with the fact that inner shell replacement by a pseudopotential provides an opportunity to better describe the outer shells involved in the chemical bond, i.e. to use more diffuse and polarization functions for their description. Calculation of the lattice structure and behavior is governed by good description of the RE ion outer shells involved in the chemical bond.

The phonon spectrum and elastic constants were also calculated during this study using the PBE0-D3 functional including the Grimme dispersion correction. Consideration of dispersion interactions through the Grimme correction does not improves the calculated phonon spectrum (Table 5, 6). The contribution of the Grimme correction is equal to 0.005% of the energy per cell.

Calculation of the elastic constants with the Grimme correction (Table 7) negligibly improves the agreement with the experimental data, whereby the calculation time increases significantly (by $\sim 20\%$).

Thus, for calculation of the crystalline structure, phonon spectrum, elastic properties of $Gd_2Sn_2O_7$, the RE ion inner shells up to $4f$, inclusive, may be replaced by a pseudopotential. Utilization of the pseudopotential for gadolinium to replace the inner shells up to $4f$, inclusive, and the hybrid PBE0 functional will make it possible to describe adequately a set of properties of $Gd_2Sn_2O_7$ — crystal lattice, band structure, phonon spectrum, elastic properties with minimum computational burden, which is important for simulation of complex compounds with RE ion sublattice.

This study used the hybrid PBE0 functional and the quasi-relativistic ECP53MWB pseudopotential replacing the gadolinium inner shell up to $4f$, inclusive, to calculate the phonon spectrum of $Gd_2Sn_2O_7$ in the Γ-point. Its elastic properties were calculated. The effect of hydrostatic compression on fundamental vibration frequencies and elastic properties was investigated.

Table 6. Raman modes $Gd_2Sn_2O_7$

Type	Experiment [17]	Calculation		
		$4f$-shell explicitly considered		$4f$-shell replaced by a pseudopotential
		(PBE0)	(PBE0-D3)	(PBE0)
F_{1u}	105	120	122	106
F_{1u}	140	163	166	140
F_{1u}	215	229	235	210
F_{1u}	320	353	358	325
F_{1u}	390	402	413	354
F_{1u}	435	493	504	427
F_{1u}	630	645	663	627
Mean difference with experiment, %		9.5	11.8	2.3

Table 7. Elastic constants and bulk modulus (GPa) of $Gd_2Sn_2O_7$. The Grimme correction is included in the calculation with the PBE0-D3 functional

Elastic constant	Experiment [15]	Calculation		
		$4f$-shell considered explicitly		$4f$-shell replaced by a pseudopotential
		(PBE0)	(PBE0-D3)	(PBE0)
C_{11}	334	332	341	313
C_{12}	122	110	116	110
C_{44}	106	103	107	98
Mean difference with experiment, %		4.4	2.7	7.8
B	193	184	191	177

Table 8. Frequencies and types of phonon modes in the Γ-point. $Gd_2Sn_2O_7$. Ions involved in this mode are given

Frequency, cm^{-1}		Type	IR		Raman		Involved ions
calculation	experiment [17,18]		active/ inactive	intensity, km/mol	active/ inactive	intensity, rel. units	
67	–	F_{2u}	I	0	I		Gd^S
102	–	E_u	I	0	I		Gd^S, Sn
106	105	F_{1u}	A	493	I		Gd, Sn, O1, $O2^W$
140	140	F_{1u}	A	266	I		Gd, $O1^W$, O2
162	–	F_{2u}	I	0	I		Sn^S, O1
183	–	E_u	I	0	I		Gd^W, Sn, $O1^S$
210	215	F_{1u}	A	2744	I		Sn, O1
244	–	B_u	I	0	I		Gd, Sn^W
248	–	F_{1g}	I	0	I		$O1^S$
278	–	B_u	I	0	I		Gd^W, Sn
302	–	F_{2u}	I	0	I		$O1^S$
310	310	F_{2g}	I	0	A	1000	$O1^S$
325	320	F_{1u}	A	921	I		Sn^W, $O1^S$
349	348	E_g	I	0	A	78	$O1^S$
354	390	F_{1u}	A	8052	I		Sn^W, O1, $O2^S$
413	–	E_u	I	0	I		Sn^W, $O1^S$
416	415	F_{2g}	I	0	A	312	O1, $O2^S$
427	435	F_{1u}	A	1036	I		Sn^W, $O1^S$, $O2^S$
486	–	B_u	I	0	I		O1
506	502	A_g	I	0	A	895	O1
541	535	F_{2g}	I	0	A	131	O1, $O2^S$
551	–	F_{1g}	I	0	I		$O1^S$
627	630	F_{1u}	A	2958	I		$O1^S$
706	–	F_{2u}	I	0	I		$O1^S$
742	741	F_{2g}	I	0	A	71	O1

Note. Superscripts „S“ and „W“ in the last column designate strong and weak involvement of an ion in a mode, respectively. If the displacement is greater than or equal to 0.02 Å, it is designated as „S“; if the displacement is 0.005−0.01 Å, it is designated as „W“; if the displacement is lower than < 0.005 Å, an ion is not mentioned in the „Involved ions“ column.

4. Results

$Gd_2Sn_2O_7$ has phonon modes in the Γ-point typical for the pyrochlore structure:

$$\Gamma = A_{1g} + E_g + 2F_{1g} + 4F_{2g} + 3A_{2u} + 3E_u + 8F_{1u} + 4F_{2u}.$$

Six modes — $A_{1g} + E_g + 4F_{2g}$ — Raman active. Among eight F_{1u} symmetry modes, there is one translation mode and seven active modes in the IR spectrum. $2F_{1g}$, $3A_{2u}$, $3E_u$, $4F_{2u}$ modes are not active either in the IR spectra or RS spectra, they are „silent“ modes. Calculated phonon modes in the Γ-point are listed in Table 8. From the analysis of displacement vectors calculated *ab initio*, the degree of ion involvement into each mode was derived (the „Involved ions“ column in Table 8). Ionic displacements in phonon modes are shown in Figure 5.

The gadolinium ion in the F_{2u} ($67\,cm^{-1}$) symmetry mode and the oxygen ions in the F_{2u} ($302\,cm^{-1}$) symmetry mode and F_{1u} ($354\,cm^{-1}$) symmetry mode have the maximum displacements of ~ 0.04 ÅIf the displacement is greater than or equal to 0.02 Å, it is designated as „S“ (Strong), if the displacement is 0.005 − 0.01 Å, it is designated as „W“ (Weak), if the displacement is lower than < 0.005 Å, an ion is not mentioned in the „Involved ions“ column, Table 8. According to the calculations (Figure 5), the gadolinium ions are involved in modes with frequencies up to $250\,cm^{-1}$, tin — is involved in mode with frequencies up to $\sim 450\,cm^{-1}$. Oxygen involvement is present throughout the frequency range, this is applicable, in particular, to ions in the $48f$ (O1) position. Modes in which only oxygen ions are involved and modes in which oxygen ions are primarily involved may be distinguished. Only oxygen ions are involved in all RS modes. The E_g ($349\,cm^{-1}$) and A_g ($506\,cm^{-1}$) symmetry modes involve only the oxygen ions in the $48f$ (O1) position. According to the calculations (Table 8), the F_{2g} ($310\,cm^{-1}$) symmetry mode

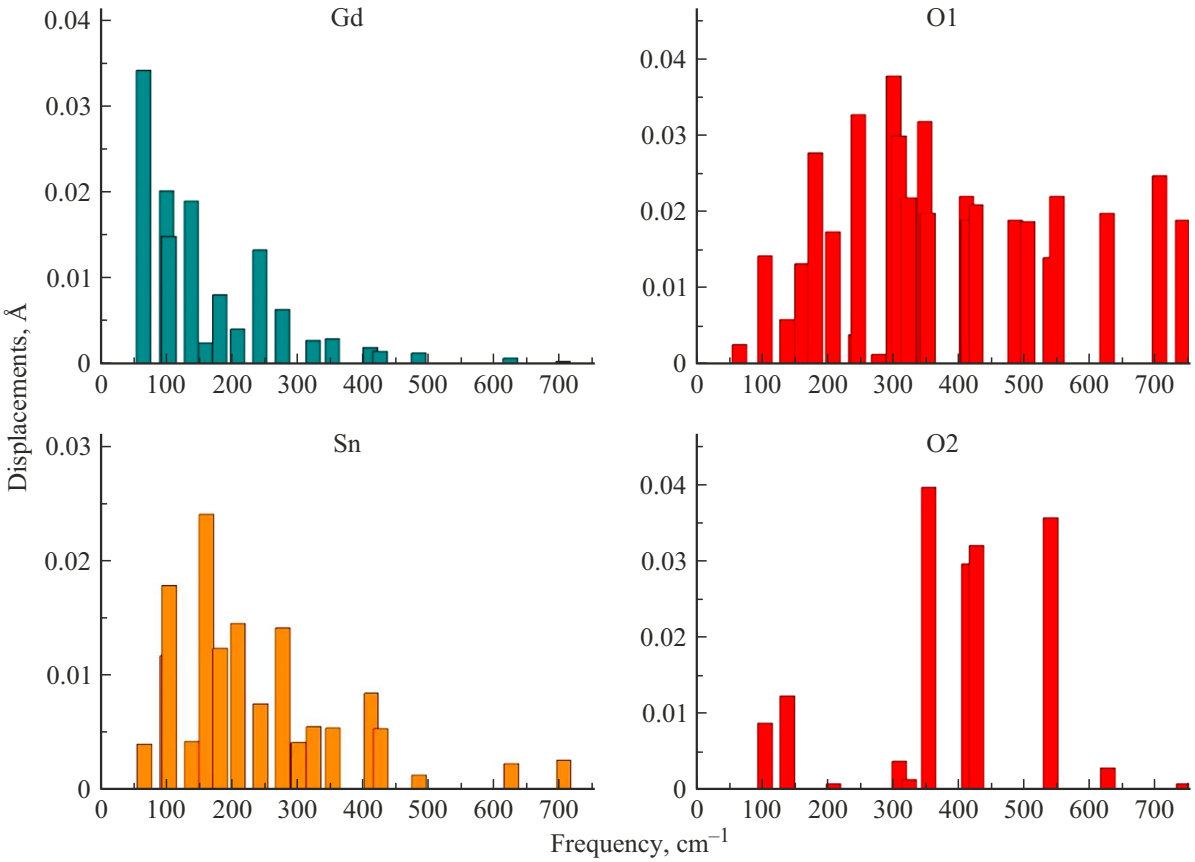

Figure 5. Displacements of ions in the phonon modes of $Gd_2Sn_2O_7$.

is the most intense RS mode, where the oxygen ions in the $48f$ (O1) position are primarily involved. The A_g (506 cm^{-1}) symmetry mode that involves only the O1 ions is similar to it in intensity. Thus, the frequency variation of two most intense RS modes — F_{2g} (310 cm^{-1}) and A_g (506 cm^{-1}) — may suggest coordinate variation of the oxygen atoms in the $48f$ position.

The most intense F_{1u} (354 cm^{-1}) symmetry IR mode primarily involves the oxygen ions with strong involvement of ions in the $8b$ (O2) position. The F_{1u} (627 cm^{-1}) symmetry IR mode with the maximum frequency primarily involves the oxygen ions in the $48f$ position. The F_{2g} (742 cm^{-1}) symmetry IR mode with the maximum frequency primarily involves the oxygen ions in the $48f$ position, but the intensity of this mode is low (Table 8). The calculations (Figure 5) predict the mixture of vibrations of structural units. The IR modes involve all ions — gadolinium, tin and oxygen, but in different degrees. Significant involvement of gadolinium and tin in the low-frequency „silent“ modes that are inactive either in the IR or RS spectra (Table 8). Note that the calculation is in good agreement with the available experimental data.

The study investigated the hydrostatic compression effect on $Gd_2Sn_2O_7$. The calculations predict that the mechanical stability conditions [32] for the pyrochlore structure are fulfilled within 0–12 GPa (Table 9). According to the experimental data [18], the pyrochlore structure remains within this pressure range. The lattice constant and band gap at different pressures are shown in Table 10. According to the calculations, BG in compression to 12 GPa varies negligibly.

The calculated phonon spectra in the Γ-point in hydrostatic compression are listed in Table 11. Dependence of each mode frequency on pressure was approximated by the straight line $Y = ax + b$. Table 11 shows the coefficients a and b of this dependence.

The calculations predict that the high-frequency modes F_{1g}, F_{1u}, F_{2u}, F_{2g} with frequencies within 550–740 cm^{-1} respond most strongly to the hydrostatic compression. The low-frequency modes involving the gadolinium and tin ions (E_u, F_{1u}, F_{2u} with frequencies up to 160 cm^{-1}) vary least of all when pressure is applied. In general, the angular frequency-pressure coefficient a (cm^{-1}/GPa) is from 1 to 2 for modes with frequencies up to 325 cm^{-1}, from 2 to 3 for modes with frequencies up to 350–540 cm^{-1} and about 5 cm^{-1}/GPa for modes with frequencies higher than 550 cm^{-1} (these are the last four modes).

The calculated elastic constants and moduli of elasticity in hydrostatic compression are listed in Table 12. Dependence

Table 9. Conditions of mechanical stability in hydrostatic pressure for $Gd_2Sn_2O_7$

P, GPa	Elastic constants, GPa	Mechanical stability conditions	Left-hand side value
0	$C_{11} = 319$	$C_{11} + 2C_{12} + P > 0$	543
	$C_{12} = 112$	$C_{11} - C_{12} - 2P > 0$	207
	$C_{44} = 98$	$C_{44} - P > 0$	98
3	$C_{11} = 334$	$C_{11} + 2C_{12} + P > 0$	581
	$C_{12} = 122$	$C_{11} - C_{12} - 2P > 0$	206
	$C_{44} = 103$	$C_{44} - P > 0$	100
6	$C_{11} = 348$	$C_{11} + 2C_{12} + P > 0$	616
	$C_{12} = 131$	$C_{11} - C_{12} - 2P > 0$	205
	$C_{44} = 108$	$C_{44} - P > 0$	102
9	$C_{11} = 362$	$C_{11} + 2C_{12} + P > 0$	649
	$C_{12} = 139$	$C_{11} - C_{12} - 2P > 0$	205
	$C_{44} = 112$	$C_{44} - P > 0$	103
12	$C_{11} = 375$	$C_{11} + 2C_{12} + P > 0$	683
	$C_{12} = 148$	$C_{11} - C_{12} - 2P > 0$	203
	$C_{44} = 116$	$C_{44} - P > 0$	104

Table 10. Lattice constant and band gap of $Gd_2Sn_2O_7$ in hydrostatic compression

P, GPa	Lattice constant, Å	Band gap, eV
0	10.52	5.4
3	10.46	5.5
6	10.41	5.7
9	10.36	5.8
12	10.32	5.9

of each elastic constant on pressure was approximated by the straight line $Y = ax + b$. Its coefficients a and b are listed in Table 12. The calculations predict that C_{11} varies most strongly with pressure — the angular coefficient a for it is equal to ~ 5, while for this coefficient is$C_{44} \sim 1.6$ GPa/GPa. Different elastic constant-to- pressure dependence agrees with the fact that, according to the calculations, a part of bonds in the $Gd_2Sn_2O_7$ crystal is close to the ionic bond, another part is covalent. Thus, the charge on the Gd-O bond is by an order of magnitude lower than that on the Sn-O bond (Table 13).

5. Conclusion

This study used the *ab initio* calculation within the MOLCAO approach to determine the frequencies and types of fundamental vibrations of $Gd_2Sn_2O_7$. From the analysis of displacement vectors calculated *ab initio*, the degree of ion involvement into each mode was derived. Modes with absolute or primary involvement of oxygen in the $48f$ position characterized by the x coordinate were identified. They include most intense RS modes. Thus, the frequency variation of two most intense $F2g$ ($310\,cm^{-1}$) symmetry and A_g ($506\,cm^{-1}$) symmetry RS modes may suggest coordinate variation of the oxygen atoms in the $48f$ position when the crystal is under external exposure. It

Table 11. $Gd_2Sn_2O_7$. Phonon frequencies in the Γ-point at hydrostatic pressure

Frequency, cm^{-1}						$Y = ax + b$		Involved ions
P, GPa	0	3	6	9	12	b	a	
F_{2u}	67	73	78	81	84	68.2	1.40	Gd^S
E_u	102	104	104	105	104	102.8	0.17	Gd^S, Sn
F_{1u}	106	110	112	115	116	106.8	0.83	Gd, Sn, O1, $O2^W$
F_{1u}	140	142	145	148	150	139.8	0.87	Gd, $O1^W$, O2
F_{2u}	162	165	167	169	171	162.4	0.73	Sn^S, O1
E_u	183	188	194	199	204	183.0	1.77	Gd^W, Sn, $O1^S$
F_{1u}	210	214	219	224	228	209.8	1.53	Sn, O1
B_u	244	250	256	261	265	244.6	1.77	Gd, Sn^W
F_{1g}	248	255	261	268	274	248.2	2.17	$O1^S$
B_u	278	283	287	291	294	278.6	1.33	Gd^W, Sn
F_{2u}	302	308	314	322	329	301.4	2.27	$O1^S$
F_{2g}	310	318	325	333	338	310.6	2.37	$O1^S$
F_{1u}	325	328	332	335	341	324.4	1.30	Sn^W, $O1^S$
E_g	349	358	367	374	381	349.8	2.67	$O1^S$
F_{1u}	354	366	377	388	396	355	3.53	Sn^W, O1, $O2^S$
E_u	413	421	430	438	446	413	2.77	Sn^W, $O1^S$
F_{2g}	416	425	434	443	450	416.4	2.87	O1, $O2^S$
F_{1u}	427	437	447	457	465	427.4	3.2	Sn^W, $O1^S$, $O2^S$
B_u	486	493	499	505	511	486.4	2.07	O1
A_g	506	514	523	530	538	506.2	2.67	O1
F_{2g}	541	551	560	571	578	541.4	3.13	O1, $O2^S$
F_{1g}	551	567	583	597	611	551.8	5	$O1^S$
F_{1u}	627	642	657	672	685	627.4	4.87	$O1^S$
F_{2u}	706	723	740	755	771	706.6	5.4	$O1^S$
F_{2g}	742	757	772	787	800	742.4	4.86	O1

Table 12. elastic constants of $Gd_2Sn_2O_7$ at hydrostatic pressure (GPa). Moduli of elasticity (Hill), Poison's ratio and Vickers hardness (GPa) are also provided

P, GPa	0	3	6	9	12	b	a
C_{11}	319	334	348	362	375	319.3	4.77
C_{12}	112	122	131	139	148	112.5	3.0
C_{44}	98	103	108	112	116	98.2	1.57
Bulk modulus,B	181	192	203	214	224	181	3.67
shear modulus, G	100	104	108	112	115	100	1.33
EYoung's modulus,	253	264	275	285	294	253.2	3.57
Poisson's ratio	0.27	0.27	0.27	0.28	0.28	0.268	0.001
	12.2	12.3	12.4	12.4	12.4	12.22	0.023
Vickers hardness H_V							

Table 13. Ion charges and charges on bonds of $Gd_2Sn_2O_7$ (Mulliken), $|e|$

Gd	Sn	O1	O2	Gd-O1	Gd-O2	Sn-O1
+2.249	+1.928	−1.128	−1.584	0.012	0.062	0.149

is shown that, when hydrostatic compression is applied, the high-frequency modes F_{1g}, F_{1u}, F_{2u}, with frequencies $550-740\,cm^{-1}$ that primarily involve the oxygen ions in the $48f$ position vary most strongly. It is shown that the elastic constants C_{11}, C_{12} and C_{44} of gadolinium stannate respond differently to the applied hydrostatic compression. When the hydrostatic pressure is applied, they increase is from 1.6 (C_{44}) to 4.8 GPa (C_{11}) per 1 GPa of the applied pressure.

Funding

The study was supported by the Ministry of Education and Science of the Russian Federation (project № FEUZ-2023-0017). The study was carried out under the state assignment of the Ministry of Education and Science of the Russian Federation (topic „Quantum“,
No 122021000038-7). The „Uran“ supercomputer provided by IMM of the Ural Branch of RAS was used to perform the investigations.

Conflict of interest

The authors declare that they have no conflict of interest.

References

[1] M.A. Subramanian, G. Aravamudan, G.V. Subba Rao. Prog. Solid St. Chem., **15** (2), 55 (1983). DOI: 10.1016/0079-6786(83)90001-8
[2] R. Zhang, Q. Xu, W. Pan, C.L. Wan, L.H. Qi, H.Z. Miao. Key Eng. Mater., **336–338**, 420 (2007). DOI: 10.4028/www.scientific.net/kem.336-338.420
[3] D.R. Clarke. Surf. Coat. Technol., **163**, 67 (2003). DOI: 10.1016/S0257-8972(02)00593-5
[4] J.W. Fergus. Metall. Mater. Trans. E, **1** (2), 118 (2014). DOI: 10.1007/s40553-014-0012-y
[5] K.E. Sickafus. Science, **289**, 748 (2000). DOI: 10.1126/science.289.5480.748
[6] J. Lian, R.C. Ewing et al. J. Mater. Res., **19**, 1575 (2004). DOI: 10.1557/JMR.2004.0178
[7] R. Cao, G. Quan, Z. Shi, T. Chen, Z. Luo, G. Zheng, Z. Hu. J. Phys. Chem. Solids., **118**, 109 (2018). DOI: 10.1016/j.jpcs.2018.03.002
[8] A.M. Srivastava. Opt. Materials, **31** (6), 881 (2009). DOI: 10.1016/j.optmat.2008.10.021.
[9] S.A. Klimin, M.N. Popova, E.P. Chukalina, B.Z. Malkin, A.R. Zakirov, E. Antic-Fidancev, Ph. Goldner, P. Aschehoug, G. Dhalenne. Phys. Solid State, **47** (8), 1425 (2005). DOI: 10.1134/1.2014481.
[10] D. Jina, X. Yu, H. Yang, H. Zhu, L. Wang, Y. Zheng. J. Alloys Compd., **474**, 557 (2009). DOI: 10.1016/j.jallcom.2008.06.159
[11] A.A. Saleh, H.Z. Hamamera, H.K. Khanfar, A.F. Qasrawi, G. Yumusak. Mat. Sci. Semicond. Proc., **88**, 256 (2018). DOI: 10.1016/j.mssp.2018.08.017
[12] K.W. Li, H. Li, H. Zhang, R. Yu, H. Wang, H. Yan. Mater. Res. Bull., **41**, 191 (2006). DOI: 10.1016/j.materresbull.2005.07.018
[13] R.A. McCauley, F.A. Hummel. J. Lumin., **6** (2), 105 (1973). DOI: 10.1016/0022-2313(73)90046-x
[14] S. Fujihara, K. Tokumo. Chem. Mater., **17**, 22 (2005). DOI: 10.1021/cm0513785
[15] J. Feng, B. Xiao, Z.X. Qu, R. Zhou, W. Pan. Appl. Phys. Lett., **99**, 201909 (2011). DOI: 10.1063/1.3659482
[16] L.T. Denisova, Yu.F. Kargin, V.M. Denisov. Neorgan. mater, **53** (975), 2017 (in Russian). DOI: 10.7868/S0002337X17090111
[17] M.T. Vandenborre, E. Husson, J.P. Chatry, D. Michel. J. Raman Spectrosc., **14**, 63 (1983). DOI: 10.1002/jrs.1250140202
[18] K.M. Turner, C.L. Tracy, W.L. Mao, R.C. Ewing. J. Phys.: Condens. Matter., **29**, 504005 (2017). DOI: 10.1088/1361-648X/aa9960
[19] R. Pei, B. Lu, Y. Dong, B. You. Acta Materialia, **270**, 119868 (2024). DOI: 10.1016/j.actamat.2024.119868
[20] J. Liao, L. Kong, Q. Wang, J. Li, G. Peng. J. Adv. Opt. Photon., **1** (2), 95 (2018). DOI: 10.32604/jaop.2018.02756
[21] R. Dovesi, V.R. Saunders, C. Roetti, R. Orlando, C.M. Zicovich-Wilson, F. Pascale, B. Civalleri, K. Doll, N.M. Harrison, I.J. Bush, Ph. D'Arco, M. Llunel, M. Causa, Y. Noel, L. Maschio, A. Erba, M. Rerat, S. Casassa. CRYSTAL17 User's Manual [Electronic source]. URL: http://www.crystal.unito.it/index.php
[22] F. Cora. Mol. Phys., **103** (18), 2483 (2005). DOI: 10.1080/00268970500179651
[23] G. Sophia, P. Baranek, C. Sarrazin, M. Rerat, R. Dovesi. *Systematic influence of atomic substitution on the phase diagram of ABO_3 ferroelectric perovskites* (2014) [Electronic source]. URL: http://www.crystal.unito.it/Basis_Sets/tin.html
[24] *Energy-consistent Pseudopotentials of the Stuttgart* [Electronic source]. URL: http://www.tc.uni-koeln.de/PP/clickpse.en.html.
[25] F. Pascale, C.M. Zicovich-Wilson, F. Lopez Gejo, B. Civalleri, R. Orlando, R. Dovesi. J. Comput. Chem., **25**, 888 (2004). DOI: 10.1002/jcc.20019
[26] R. Dovesi, R. Orlando, A. Erba, C.M. Zicovich-Wilson, B. Civalleri, S. Casassa, L. Maschio, M. Ferrabone, M. De La Pierre, P. D'Arco, Y. Noel, M. Causa, M. Rerat, B. Kirtman. Int. J. Quantum Chem., **114**, 1287 (2014). DOI: 10.1002/qua.24658
[27] L. Maschio, B. Kirtman, R. Orlando, M. Rerat. J. Chem. Phys., **137** (20), 204113 (2012). DOI: 10.1063/1.4767438
[28] P. Labeguerie, F. Pascale, M. Merawa, C. Zicovich-Wilson, N. Makhouki, R. Dovesi. Eur. Phys. J. B, **43**, 453 (2005). DOI: 10.1140/epjb/e2005-00078-6
[29] T.M. Duarte, P.G.C. Buzolin, I.M.G. Santos, E. Longo, J.R. Sambrano. Theor. Chem. Accounts, **135** (6), 150 (2016). DOI: 10.1007/s00214-016-1901-1
[30] Y. Tian, B. Xu, Z. Zhao. Int. J. Refract. Hard. Met., **33**, 93 (2012). DOI: 10.1016/j.ijrmhm.2012.02.021
[31] D.V. Korabel'nikov, Y.N. Zhuravlev. Phys. Solid State, **58** (6), 1166 (2016). DOI: 10.1134/S106378341606025.
[32] Yu.Kh. Vekilov, O.M. Krasilnikov. UFN, **179** (8), 883 (2009) (in Russian). DOI: 10.3367/UFNr.0179.200908f.0883

Translated by E.Ilinskaya